Study of the systematic fully grouted rock bolts performance in tunnels considering installation condition of bolt head

Study of the systematic fully grouted rock bolts performance in tunnels considering installation condition of bolt head

Mauro Giordanella [1], Masoud Ranjbarnia [2, *], Pierpaolo Oreste [3], Milad Zaheri [4]

[1] *M.Sc, Department of Environmental, Land and Infrastructure Engineering, Politecnico di Torino, Turin, Italy.* *m.giordanella@live.it*

[2] *Associate Professor, Department of Geotechnical Engineering, Faculty of Civil Engineering, University of Tabriz, Tabriz, Iran. orcid.org/0000-0003-3995-3258* *M.ranjbarnia@tabrizu.ac.ir*

[3] *Professor, Department of Environmental, Land and Infrastructure Engineering, Politecnico di Torino, Turin, Italy. orcid.org/0000-0001-8227-9807* *Pierpaolo.oreste@polito.it*

[4] *Ph.D student, Department of Geotechnical Engineering, Faculty of Civil Engineering, University of Tabriz, Tabriz, Iran. orcid.org/0000-0002-9619-9397* *Miladzaheri@tabrizu.ac.ir*

Corresponding author:

Masoud Ranjbarnia

E-mail: m.ranjbarnia@tabrizu.ac.ir

Tel: +989144022676

Study of the systematic fully grouted rock bolts performance in tunnels considering installation condition of bolt head

A two-dimensional parametric numerical study is conducted to investigate some unknown aspects of the systematic fully grouted rock bolts performance in the stability of tunnels. The influence of the bolt head constraint conditions i.e., a stiff steel plate on a smooth rigid basement or a rough basement (the rigid and flexible complexes, respectively) on the convergence confinement, development of the plastic band, and the maximum bolt force is studied in a tunnel located in a poor or good rock mass quality. As well, the difference of the tunnel convergence on the bolt head location and in the middle between two bolts is the other investigated parameter. The results show that for a tunnel excavated in a poor rock mass quality at great depths (very squeezing condition), the difference of convergences must be considered particularly for large openings in which the spacing of the bolts is not small.

Keywords: Grouted rock bolts; Tunnel; Convergence confinement; Bolt head constraint condition; Numerical simulation

Introduction

Due to the numerous advantageous benefits of grouted rock bolts in underground openings, their usage has been widely increased in practice. Accordingly, a great number of studies by the analytical, numerical, and experimental methods have been conducted to explore various aspects of rock bolts performance in rock masses including systematic or random discontinuities.

Regarding studies associated to tunnel stability by systematic radial bolting, the analytical approaches have investigated fundamental parameters of bolting and identified the most critical ones.

Farmer (1975) obtained the shear stress distribution along a fully grouted rock bolt due to the bonding between the rock bolt and grout. The interaction between the grouted rock bolt and surrounding rock mass was studied by Fahimifar and Soroush (2005), Indraratna and Kaiser (1990 a, b), Cai et al. (2004 a, b), and Ghadimi et al. (2015).

Peila and Oreste (1995) and Oreste and Peila (1996) determined the force distribution along a bolt considering both the ideal and real connection between the bolt and the grout, and finally, obtained the GRC of the reinforced tunnel. In this manner, the behavior of the bolt end-plate force-displacement was considered. Li and Stillborg (1999) improved the previous researches and developed a method in which the interaction between the rock bolt and the grout (in the case of the grouted rock bolts) or between the rock bolt and the rock mass (in the case of the frictionally coupled bolts) was modeled. Also, the effect of the existence of shotcrete layer (Stille et al. 1989), the bolting density (number of bolts per unit area) (Pelizza et al. 1995; Oreste 2004, 2008, 2009, 2013; Osgoui and Oreste 2007, 2010; Oreste and Cravero 2008; Carranza-Torres 2009), the pre-tensioned bolt (Ranjbarnia et al. 2014, 2015; Bobet and Einstein 2011), bolt head constraint condition (Fahimifar and Ranjbarnia 2009), the existence of a joint plane in the rock mass (Liu and Li 2017), and the viscoelastic behaviour of rock mass (Wu et al. 2019) has been investigated.

However, all of the efforts result in a uniform convergence of the tunnel wall, which is not the case in practice. That is, due to less contribution in farther distances from a bolt location, the corresponding inward radial displacements are greater than those in the bolt head location. Ranjbarnia et al. (2016) simulated the contribution of a bolt within its domain of influence as a radial pressure with an exponential trend, but they did not present a method to obtain the non-uniform displacements of the tunnel wall.

One of the aspects which has not been much addressed is the influence of the bolt head constraint condition. That is, few studies have considered this issue. However, in these researches, the distribution of forces along a bolt has been investigated and the tunnel convergence has not addressed.

Due to inherent limitations associated with the analytical approaches, on the other hand, some numerical studies have been simultaneously carried out to explore some other issues of bolting performance as follows:

- Those related to the tunnel, rock mass, and loading conditions e.g. non-circular tunnel section and non-hydrostatic in-situ stress condition (as an example: a parametric study to evaluate the influence of various shapes of underground openings as well as horizontal in-situ stress to estimate the required bolt length in the roof and wall of the tunnel (Teymen 2017)), presence of systematic discontinuities (i.e., joint sets) in rock mass and their properties (can be found in

references (Nie et al. 2014, 2018)), working condition (Zhang et al. 2008, Xu et al. 2010), and applying of dynamic loading (Mortazavi and Tabatabaei Alavi, 2013; Tahmasebinia et al. 2018) and so on;

- Those associated with bolt properties e.g. de-bonding in the bolt-medium interface (e.g. due to crack in the grout between the bolt and the medium) (Nemcik et al. 2014; Zhu et al. 2015; Chang et al. 2017), bolt length (Goel and Swarup 2005, Wang et al. 2012), and bolt materials (Grasselli 2005).

The laboratory tests have been also carried out to find the tensile capacity of the bolt and (or) to calibrate numerical studies (Karanam and Dasyapu 2005).

The literature review indicates that great numerous studies have been conducted on the performance of the rock bolt in tunneling. However, some other aspects of bolting have not sufficiently (say quantitatively) discussed. Therefore, they are required to be more addressed. The performance of the bolting system in poor and good quality of rock masses, the influence of bolt head constraint condition in the confinement of tunnel convergence, and the difference of tunnel convergences in the bolt head and in the middle between two bolts are investigated in this paper using the numerical method. The last issue can reflect the domain zone of influence of each bolt in different rock masses.

The developed numerical model

In the last decade, various software programs have been employed to simulate geotechnical problems. According to previously published papers as well as researchers advisement, the ABAQUS and FLAC are the most reliable software in the case of continuum media in geotechnical problems, and they are frequently used in research papers in the broad area of geotechnical engineering. This fact is more highlighted with FLAC software particularly in the case of a tunnel simulation.

On the other hand, due to the implementation of the Cable structural element in FLAC which directly simulates a bolt and considers its interaction with the medium, the authors use this software for the parametric analysis.

The set model contains 2880 quadrilateral elements. Starting from a square grid of 45x64 size, the geometry of the cavity is defined using a FISH code, which distorts the grid by joining the opposite sides and leaving a circular hollow in the middle of the dimensions of the cross-section of the tunnel. The distorted grid representing the geometry of the problem is shown in Figure 1. Noted that FISH is a programming

language embedded within FLAC that enables the user to define new variables and functions. These functions may be used to extend FLAC's usefulness or add user-defined features. For example, special grid generators may be implemented, and parameter studies may be automated (Itasca 2012).

[Figure 1 near here]

The dimensions of the model have been chosen to ignore the effects of the edges on the calculation results (i.e., stresses and strains around the opening) (Zaheri et al. 2020 a , b; Ranjbarnia et al. 2020).

It is assumed that a homogeneous and an isotropic medium is subjected to hydrostatic pressure (i.e., $k_0 = 1$). In this way, it is possible to simulate the lithostatic pressure presented prior to the tunnel excavation by applying a certain uniform pressure to the model (P_0).

At first, a pressure (P_i) equal to the lithostatic pressure (P_0) is assigned to the walls of the cavity which equals to the). In this condition, the excavation face is still very far from the studied section (i.e., the removal of material does not affect this section). After a preliminary calculation, which models the elastic conditions, the excavation stages are simulated.

The progress of the excavation phases (Figure 2) is simulated by gradually reducing the internal pressure from the lithostatic value to the null value:

- $P_i = P_0$: when the excavation face is far from the studied section (case a);
- $P_i = 0.6P_0$ (as an assumption): when the excavation face reaches the studied section (case c);
- $P_i = 0$: when the excavation face has passed a certain distance, about two diameters of the tunnel from the studied section (the case e).

In correspondence of the frontal side of the excavation, when it passes beyond the studied section up to a certain distance (about two tunnel diameter), the applied internal pressure is not zero; but the presence of the rock mass at the excavation face still applies some support counterforce to the walls.

The installation of the bolts takes place in correspondence of the face when the internal pressure $P_i = 0.6P_0$ is present. The bolts are simulated as the mono-dimensional elements connected to the grid elements in such a way to simulate the real constraint condition. A schematic representation of the case of the study is reported in Figure 3.

[Figure 2 near here]

[Figure 3 near here]

The parameters and the input data considered in this study

In the FLAC code manual (Itasca 2012), the stresses in the plastic zone obey the modified Hoek-Brown failure criterion (Hoek et al. 2002) while the stress-strain relationship is the elastic-perfectly-plastic. The relationship between the major and minor principal stresses (σ_1 and σ_3, respectively) is as follows:

$$\sigma_1 = \sigma_3 + \sigma_{ci}\left(m_b \frac{\sigma_3}{\sigma_{ci}} + s\right)^a \quad (1)$$

where σ_{ci} is the uniaxial compressive strength of the intact rock; m_i is the constant parameter; m_b , s and a are the rock mass constants defined as a function of the GSI (Geological Strength Index) and the disturbance coefficient (D) as follows (Hoek et al. 2002):

$$m_b = m_i e^{\frac{GSI-100}{28-14D}} \quad (2)$$

$$s = e^{\frac{GSI-100}{9-3D}} \quad (3)$$

$$a = 0.5 + \frac{1}{6}\left(e^{-\frac{GSI}{15}} - e^{-\frac{20}{3}}\right) \quad (4)$$

Table 1 shows the 12 basic cases obtained by combining four types of rock masses defined by four different GSI values, and three initial lithostatic pressures (P_0) (corresponding to three different tunnel depths). In all cases, the rock mass density has been set equal to $\gamma = 0.0245\ \frac{\mathrm{MN}}{\mathrm{m}^3}$. From this value, we can trace back to the depth of the tunnel (H_{tunnel}).

[Table 1 near here]

However, the rock mass, after the elastic behavior, may follow different patterns of stress-strain behavior depending on the quality of the rock mass (Alejano et al. 2010; Zaheri et al. 2019, Zaheri and Ranjbarnia 2020, 2021). The analyses are conducted following two paths:

- For the cases with low values of GSI, typical of the poor rock mass quality, it is assumed that rock mass has the Elastic-Perfectly-Plastic behavior. Hence, the parameters of the strength criterion (m_b and s in particular) do not significantly change in the plastic regime.
- For the cases with high values of GSI (the good rock masses quality), the Elastic–Brittle-Plastic behavior is employed. In this case, the Hoek-Brown strength

parameters considerably change to residual values once passed the elastic limit. To implement this behavior in the Hoek-Brown model in FLAC^{2D}, a FISH code was used.

It is, therefore, necessary to calculate the parameters m^{res} and s^{res} (residual values of m_b and s, respectively), and set up a code that respects this principle. These parameters were calculated with the same formulas used for the calculation of peak parameters but considering a residual value of GSI. Table 2 gives a framework to estimate the GSI^{res} from its corresponding value before failure (GSI^{peak}) (Cai et al. 2007).

[Table 2 near here]

The used characteristic parameters of the rock mass are reported in Table 3. Also, the following other parameters are assumed as fixed values: the Poisson's ratio $v = 0.25$ and the Hoek-Brown parameters $a = 0.5$, $m_i = 7$, and $D = 0$.

[Table 3 near here]

Note that the non-associated flow rule was used in the calculations through introducing the dilation angle to the rock mass. For poor rock mass qualities, this value is equal to zero, while for good rock mass qualities, it is $\frac{\emptyset}{4}$. It should be noted that $\emptyset$ is the equivalent friction angle of the rock mass (Hoek and Brown 1997).

After simulating the 12 basic cases in the absence of reinforcement, these have been associated with 2 different bolting patterns to give 24 cases. In Table 4, the two bolting arrangement patterns are shown as B_1 and B_2.

[Table 4 near here]

As the analyses are performed in the two-dimensional plane strain condition, a unit length of the tunnel (i.e., 1 m) along its axis is considered. That is, a two-dimensional analysis of a tunnel assumes the mechanical effect of the rock bolts to be spread along the unit length as cases B_1, or it must be calibrated according to the longitudinal spacing of bolt (e.g. for the cases B_2, the mechanical properties should be multiplied by two). Table 5 gives the calculated parameters of the bolting system.

[Table 5 near here]

In this table, $\emptyset_m$ is the friction angle of the grout, A_{bolt} is the cross-sectional area of the steel element, P_{exp} is the exposed perimeter calculated considering the outer radius of the bolt element (assuming that the failure occurs at the grout/rock interface), and k_m and S_m are the stiffness and the cohesive strength of the grout, respectively. Also, E_{steel} is the Elasticity Modulus of steel, and R_t is the tensile strength of the bolt element.

These 24 cases were investigated in 2 different head constraint conditions called *BH* and *FH*. *BH* acronym indicates a Bound Head condition meaning that the anchor plate used on the tunnel wall is made perfectly and has adequate rigidity (i.e., a stiff plate is tightened to the bolt head, and the complex of nut, washer, and plate are perfectly placed on a smooth basement). However, *FH* indicates a Free Head condition, no contribution of the anchor plate, and the plate is not properly leaned on the tunnel wall. The first condition was simulated by matching the node corresponded to the bolt head with the element node of the grid. The second requirement was achieved by defining the coordinates of the head independently to the grid nodes.

At first, the tunnel radius R_T and the length of bolts is considered equal to 3 m and 4 m, respectively. Also, these values are doubled in the next analyses, and thus getting 96 case studies.

A comparison is made between the results of FLAC^{2D} and those of FLAC^{3D} software programs. For this purpose, two data sets are considered as indicated in Table 6 (the tunnel radius is taken as 5 m). Bolts spacing in both circumferential and longitudinal directions are considered equal to 1 m (Table 5). Figure 4 shows the model constructed in FLAC^{3D} software. In Table 6, the obtained results are summarized.

Because of the plane strain condition of the problem i.e.,

- the uniform loading along the tunnel axis;
- the uniform tunnel cross-section;
- homogeneous and isotropic rock mass; and
- the great length of the tunnel,

the results obtained by FLAC^{2D} are almost identical to those by FLAC^{3D}. In fact, due to the plane strain condition of the problem, it is possible to use FLAC^{2D}. Therefore, the FLAC^{2D} software is used to analyze the remaining cases because its speed for the calculations is much more than FLAC^{3D}.

However, it is obvious that if the plane strain condition does not meet, the three-dimensional calculation should be performed.

[Table 6 near here]

[Figure 4 near here]

Application of the numerical simulation to the Kielder experimental tunnel

In order to verify the validity of the conducted model (say calibrate the numerical model), a real case (regarding the Kielder Experimental Tunnel) is simulated and then a comparison is made between the measured data with those of numerical simulation.

The Kielder Experimental Tunnel was built in 1974, as part of the Kielder Water Project, in Weardale Valley (England), for the study of the most appropriate support to the realization of the main tunnel of 32 km length. The tunnel was circular of 1.65 m in radius and extended to below coverage of about 100 m, with a natural overburden value of 2.56 MPa. This tunnel was divided into 8 sections (each length of about 11 m), and in each section, different support systems were installed. However, fully resin-bonded rock bolts were only used in the second section of this tunnel (Ward et al. 1983).

In this paper, as the effects of only radial bolting are investigated, the results obtained in this section of the tunnel are considered. Measurements taken inside the tunnel for this section were:

- Radial displacement of the ground around the tunnel in 4 points (0.1 to 2, and 3 m from the wall) through multipoint extensometers;
- Deformation along the bar in 4 points along the instrumented bolts.

The rock mass properties listed in Table 7 were published by Freeman (1978) and Ward et al. (1976, 1983). The in situ characteristics of the bolting system are shown in Table 8.

[Table 7 near here]

[Table 8 near here]

In particular, it is desired to compare the in situ measurement with those of conducted modeling for the two standards behaviors (the Hoek- Brown strength criterion with the Elastic-Perfectly-Plastic and Elastic-Brittle-Plastic) and the two conditions of bolt head restraining (the head perfectly anchored to the wall (*BH*), and head free (*FH*)).

Near the wall, in section 2 of the tunnel, the in-situ convergence is about 3.5 mm. In Figure 5, the comparison is made between this convergence (green ball on the abscissa axis for the null internal pressure) and the calculated convergences from numerical modeling.

For the Kielder Experimental Tunnel, the measured displacement value is located in the mid of the two simulated model behaviors. As expected, it is closest to the model with assumptions of *FH* head restraining condition of a bolt in the medium with Elastic-Perfectly-Plastic behavior. This is because a bolt head on the tunnel wall (in the absence

of the shotcrete layer) represents *FH* condition while a poor rock mass quality usually obeys the Hoek-Brown Elastic-Perfectly-Plastic model.

[Figure 5 near here]

Parametric analysis and results

As discussed, one of the aspects which has not been addressed in the previous researches is the influence of the bolt head constraint conditions. Thus, the effects of this parameter are studied in detail. In this regard, the influence of bolt spacing (in both circumferential and longitudinal directions) is also investigated in terms of the tunnel wall convergence, and the plastic zone thickness (as the most interesting outputs).

Noting that the tunnel wall displacement in the bolt head location and in the middle between two bolts is not the same. This phenomenon will be also discussed, which is not much noticed.

The influence of the bolting density and the bolt head restraining condition

Figure 6 shows the trend of convergence in terms of GSI^{peak} and tunnel depth for the two bolting schemes (B_1 and B_2) with two conditions of head restraining (*BH* and *FH*) installed at the tunnel with R_T = 3 m.

As expected, the radial movement (u) decreases with the increasing of rock mass quality index (GSI), while it is intensified with the increasing of the lithostatic pressure (P_0). In fact, a systematic radial bolting lessens the movements of the tunnel wall in all cases but the effects of strengthening are tangible for the denser bolting pattern in the poor rock mass quality subjected to the great in-situ stress. That is, to have the efficiency of the bolting system, it is necessary to consider a high bolting density accompanied with other supporting systems (e.g. shotcrete layer). The bolt density shows the number of rock bolts per unit area of the tunnel surface. In fact, it reflects the magnitude of broken rock mass reinforcement, and is an important factor of increasing the stiffness of grouted rock bolts system.

On the other hand, the condition of the restraining head plays a significant role in the poor rock mass located at greater depths, particularly it is highlighted for lower bolting density pattern. Furthermore, in the good rock mass quality ($GSI^{peak} > 50$) even at great depth (H_{tunnel} = 490 m), this factor is not critical. When a perfect constraint from the end-plate (i.e., a complete planner contact between the bolt head and the tunnel surface) is predicted, the bolts will take higher loads at the tunnel surface in comparison with the foreseen condition in

which there is not a perfect constraint. Then, the efficiency of bolts will increase to much more confine a tunnel convergence.

[Figure 6 near here]

For the developed plastic zone, it can be seen from Figure 7 that regardless of the value of P_0, the intervention of the radial bolting reduces the spread of the plastic band. This leads to a reduction of the volume of rock that potentially will load on the final support structures. The utility of the intervention becomes tangible to lower GSI ^{peak} accompanied with higher P_0. For low values of P_0 ($P_0 \leq 4$ MPa) in rock masses with good characteristics (GSI $^{peak} \geq 65$), the plastic band is not formed and the rock mass remains in the elastic condition. As can be seen from the overlap between the trend lines for the unsupported tunnel with P_0 = 4 MPa and the supported tunnel ($B_1 - FH$) with P_0 = 4 MPa, the bolting pattern sparser, in this case, has no effect on the plastic radius, which does not happen in the case with *BH* condition. It is interesting to note the difference of the plastic thickness associated with two different conditions of the restraining bolt head plate. From this point of view, in fact, this parameter becomes decisive in some cases. In particular, a decrease of the plastic thickness can be seen passing from the *FH* to *BH* conditions (especially for the cases with low GSI ^{peak} and high P_0).

The two graphs in Figure 8 show the trend of the maximum axial force (F_{max}) that develops inside the bolt. As expected, passing from a bolting system B_1 to a denser pattern B_2, the loads are distributed to a greater number of bolts, and hence, F_{max} reduces. On the other hand, the constraint condition *BH* applies greater F_{max} to the bolt than condition *FH* (see also Table 9). The same results were obtained by previous studies (Oreste and Peila 1996; Li and Stillborg 1999; Cai et al. 2004a, b; Oreste 2008; Ranjbarnia et al. 2015, 2016) as well as by in-situ measurements (Freeman 1978). However, the smaller difference between the results of these two cases in the denser bolting pattern (B_2) may be associated with the less contribution of each bolt or the smaller tunnel convergence for this pattern. In this regard, in a poor rock mass quality at great depths, no difference can be seen, since the bolts are yield.

[Figure 7 near here]

[Figure 8 near here]

[Table 9 near here]

In the case of GSI ^{peak} = 45 and P_0 = 8 MPa, it seems that double bolting is useful. However, for the other critical cases (e.g. P_0 = 12 MPa and GSI ^{peak} = 35) where the bolt

is yielded in both bolt patterns, it should be considered that the yielding is not the final break of a bolt, and therefore, the B_2 pattern more reduces the tunnel displacement. However, in these cases, another support system has to be accompanied with the bolting system.

Based on the conducted parametric analysis, it can be said that due to excessive tensile force, the systematic radial bolting cannot be applied alone for very deep tunnels ($H_{tunnel} \geq 490$ m, $P_0 \geq 12$ MPa) excavated in poor rock masses quality ($GSI^{peak} \leq 45$).

The influence of the tunnel radius

From the graphs of Figure 9, for the condition in which the rock mass is in the plastic regime (where low values of GSI^{peak} accompanied with high values of P_0), it can be inferred that the convergence of the 6 m radius tunnel is more than two times greater compared to the 3 m radius tunnel for the same radial bolting pattern. Because, as can be observed from analytical approaches (e.g., Brown et al. 1983), the strains around tunnels are independent of tunnel radius, and in the case of hydrostatic in situ stresses, the tunnel convergence can be obtained via the tangential strain at tunnel surface multiple by tunnel radius. Therefore, both tunnels show identical strains; and hence, the greater tunnel results in more convergence.

Considering Figure 10, the increase of the tunnel diameter gives an increase of developed F_{max} on the bolts. This effect is intensified for the poor rock mass located at greater depths.

In fact, the plastic radius increases in greater openings and as a result, a larger dead load is imposed on the bolts. On the other hand, the rock blocks can more freely move in a greater opening leading the bolt to be more tensioned. However, this conclusion is not the case here, since the medium is considered as a continuum.

Comparing the graphs of Figure 11, it is interesting to note how increasing the tunnel diameter can affect the width of the plastic band. Particularly, in the poor rock masses at higher depths, a more increase rate of the plastic radius can be observed with increasing the tunnel diameter.

[Figure 9 near here]

[Figure 10 near here]

[Figure 11 near here]

Comparison between the movements of the tunnel wall at the bolt head and those recorded in the middle between two bolts

By FLAC software, it is possible to obtain displacements in different points e.g., between bolts (or say in different model grids between bolts). In these locations, the displacements are not the same, and hence, the convergence between bolts is non-uniform.

Due to the less contribution of a bolt in farther distances from its longitudinal axis, it is expected that those points on the tunnel wall converge more than the location where the bolt head is situated (Figure 12).

Therefore, a comparison is made between these convergences in four graphs in Figure 13 to visualize the influence of the bolting density and the condition of the bolt head restraining on this issue.

In all cases, when talking about the very severe squeezing condition, the difference between the displacements on the bolt head and those in middle between two bolts increases. Meanwhile, it is near to zero for the good rock masses at lower depths.

From a comparison between the two first graphs, the difference between these convergences is reduced in a denser bolting pattern (i.e., 2.5 mm with B_2 scheme against 4.5 mm with B_1 scheme). However, for another bolting pattern with a lower number of bolts, it is expected that this difference exponentially increases. This fact might be important when the bolts are accompanied with a shotcrete layer (as generally). Since, in this case, due to the non-uniform movement, a bending moment is induced on the shotcrete, which may not be insignificant by itself. The produced moment can be intensified when the in-situ stresses are non-hydrostatic.

On the other hand, passing from a condition of fixed head restraining (*BH*) to a free head (*FH*), the difference between convergences on the bolt head and at the centerline decreases. Furthermore, with the *FH* condition, the density of bolting shall not have any significant effect in this regard. This issue is investigated in the greater radius (R_T = 6 m) for *BH* condition in Figure 14. For the double tunnel radius, this difference is increased. However, this difference is not significant in the case of good rock masses located at lower depths. In the worst case (P_0 = 12 MPa and $\mathrm{GSI}^{\mathrm{peak}}$ = 35), the difference of the radial displacement is about 7 mm, compared with 4.5 mm in the case with R_T = 3 m.

[Figure 12 near here]

[Figure 13 near here]

[Figure 14 near here]

Conclusions

One of the aspects which has not been much addressed in the previous researches is the influence of bolt head constraint condition on the convergence confinement, development of the plastic radius, and the developed maximum axial force in the bolt. For this purpose, a parametric study was performed to evaluate the influence of this problem. Besides, the effect of opening size and bolt spacing on the stability of the underground opening was investigated. The distinguished results are as follows:

- Bolt head constraint condition has a significant role in poor rock masses subjected to the great in-situ stress, particularly it is highlighted when the bolt spacing is greater. Furthermore, in a good rock mass quality even at great depth, this factor is not critical. In particular, passing from the *FH* to *BH* conditions, both plastic radius and tunnel wall displacements decrease. This effect is the most visible for lower GSI and higher P_0;
- If the anchor plate used on the tunnel wall is made perfectly, a greater force develops in the bolt. Also, as the spacing between adjacent bolts is decreased, this force diminishes;
- The systematic radial bolting must be accompanied with another support system (i.e., a shotcrete layer) for very deep tunnels located in a poor rock mass quality (severe squeezing condition);
- If all of the condition except tunnel radius is same for two tunnels, the bolts installed at the tunnel with greater diameter experiences more axial force. This condition is intensified when the tunnel crosses the severe squeezing rock masses; the surrounding rock mass. Hence, in this regard, the bolting density should be sufficiently increased;
- In a poor rock mass quality at great depths, the difference between convergences on the bolt head and those in middle between two bolts is too much to be ignored. Meanwhile, it is near to zero for good rock masses at lower depths.

References

Alejano, L.*, et al.* 2010. Application of the convergence-confinement method to tunnels in rock masses exhibiting Hoek–Brown strain-softening behaviour. *International Journal*

of Rock Mechanics and Mining Sciences, 47(1), 150-160. Doi: https://doi.org/10.1016/j.ijrmms.2009.07.008.

Bobet, A. and Einstein, H. 2011. Tunnel reinforcement with rockbolts. *Tunnelling and Underground Space Technology,* 26(1), 100-123. Doi: https://doi.org/10.1016/j.tust.2010.06.006.

Brown, E. T.*, et al.* 1983. Ground Response Curves for Rock Tunnels. *Journal of Geotechnical Engineering,* 109(1), 15-39. Doi: https://doi.org/10.1061/(ASCE)0733-9410(1983)109:1(15)

Cai, M.*, et al.* 2007. Determination of residual strength parameters of jointed rock masses using the GSI system. *International Journal of Rock Mechanics and Mining Sciences,* 44(2), 247-265. Doi: https://doi.org/10.1016/j.ijrmms.2006.07.005.

Cai, Y., Esaki, T. and Jiang, Y. 2004a. An analytical model to predict axial load in grouted rock bolt for soft rock tunnelling. *Tunnelling and Underground Space Technology,* 19(6), 607-618. Doi: https://doi.org/10.1016/j.tust.2004.02.129.

Cai, Y., Esaki, T. and Jiang, Y. 2004b. A rock bolt and rock mass interaction model. *International Journal of Rock Mechanics and Mining Sciences,* 41(7), 1055-1067. Doi: https://doi.org/10.1016/j.ijrmms.2004.04.005.

Carranza-Torres, C. 2009. Analytical and numerical study of the mechanics of rockbolt reinforcement around tunnels in rock masses. *Rock mechanics and rock engineering,* 42(2), 175-228. Doi: https://doi.org/10.1007/s00603-009-0178-2.

Chang, X.*, et al.* 2017. Study on grout cracking and interface debonding of rockbolt grouted system. *Construction and Building Materials,* 135, 665-673. Doi: https://doi.org/10.1016/j.conbuildmat.2017.01.031.

Fahimifar, A. and Ranjbarnia, M. 2009. Analytical approach for the design of active grouted rockbolts in tunnel stability based on convergence-confinement method. *Tunnelling and Underground Space Technology,* 24(4), 363-375. Doi: https://doi.org/10.1016/j.tust.2008.10.005.

Fahimifar, A. and Soroush, H. 2005. A theoretical approach for analysis of the interaction between grouted rockbolts and rock masses. *Tunnelling and Underground Space Technology,* 20(4), 333-343. Doi: https://doi.org/10.1016/j.tust.2004.12.005.

Farmer, I. W. 1975. Stress distribution along a resin grouted rock anchor. *International Journal of Rock Mechanics and Mining Sciences & Geomechanics Abstracts,* 12(11), 347-351. Doi: https://doi.org/10.1016/0148-9062(75)90168-0.

Freeman, T. 1978. The behaviour of fully-bonded rock bolts in the Kielder experimental tunnel. *Tunnels & Tunnelling International,* 10(5).

Ghadimi, M., Shahriar, K. and Jalalifar, H. 2015. An Analytical Model to Predict Shear Stress Distribution in Fully Encapsulated Rock Bolts. *Geotechnical and Geological Engineering,* 33(1), 59-68. Doi: https://doi.org/10.1007/s10706-014-9820-1.

Goel, R. K., and Swarup, A. 2005. Shape of underground openings and rock bolt length. In *ISRM International Symposium-EUROCK 2005*. International Society for Rock Mechanics and Rock Engineering.

Grasselli, G. 2005. 3D behaviour of bolted rock joints: experimental and numerical study. *International journal of rock mechanics and mining sciences*, 42(1), 13-24. Doi: https://doi.org/10.1016/j.ijrmms.2004.06.003.

Hoek, E. and Brown, E. T. 1997. Practical estimates of rock mass strength. *International Journal of Rock Mechanics and Mining Sciences,* 34(8), 1165-1186. Doi: https://doi.org/10.1016/S1365-1609(97)80069-X.

Hoek, E., Carranza-Torres, C. and Corkum, B. 2002. Hoek-Brown failure criterion-2002 edition. *Proceedings of NARMS-Tac,* 1, 267-273.

Indraratna, B. and Kaiser, P. 1990a. Analytical model for the design of grouted rock bolts. *International Journal for Numerical and Analytical Methods in Geomechanics,* 14(4), 227-251. Doi: https://doi.org/10.1002/nag.1610140402

Indraratna, B. and Kaiser, P. 1990b. Design for grouted rock bolts based on the convergence control method. *International Journal of Rock Mechanics and Mining Sciences & Geomechanics Abstracts,* 27(4), 269-281. Doi: https://doi.org/10.1016/0148-9062(90)90529-B.

Itasca, 2012. Fast Lagrangian Analysis of Continua. Minneapolis: Minn: Itasca Consulting Group Inc.

Karanam, U. M. R. and Dasyapu, S. K. 2005. Experimental and numerical investigations of stresses in a fully grouted rock bolts. *Geotechnical & Geological Engineering,* 23(3), 297-308. Doi: https://doi.org/10.1007/s10706-004-9518-x.

Li, C. and Stillborg, B. 1999. Analytical models for rock bolts. *International Journal of Rock Mechanics and Mining Sciences,* 36(8), 1013-1029. Doi: https://doi.org/10.1016/S1365-1609(99)00064-7.

Liu, C.H. and Li, Y.Z. 2017. Analytical Study of the Mechanical Behavior of Fully Grouted Bolts in Bedding Rock Slopes. *Rock Mech Rock Eng,* 50(9) , 2413–2423. Doi: https://doi.org/10.1007/s00603-017-1244-9.

Mortazavi, A. and Alavi, F. T. 2013. A numerical study of the behavior of fully grouted rockbolts under dynamic loading. *Soil Dynamics and Earthquake Engineering,* 54, 66-72. Doi: https://doi.org/10.1016/j.soildyn.2013.08.003.

Nemcik, J.*, et al.* 2014. Numerical modelling of failure propagation in fully grouted rock bolts subjected to tensile load. *International Journal of Rock Mechanics and Mining Sciences,* 71, 293-300. Doi: https://doi.org/10.1016/j.ijrmms.2014.07.007.

Nie, W.*, et al.* 2014. Numerical studies on rockbolts mechanism using 2D discontinuous deformation analysis. *Tunnelling and Underground Space Technology,* 41, 223-233. Doi: https://doi.org/10.1016/j.tust.2014.01.001.

Nie, W.*, et al.* 2018. Effects of joints on the reinforced rock units of fully-grouted rockbolts. *Tunnelling and Underground Space Technology,* 71, 15-26. Doi: https://doi.org/10.1016/j.tust.2017.07.005.

Oreste, P. 2004. Designing of radial bolting in tunnels. *Journal of Mining science,* 40(4), 384-394. Doi: https://doi.org/10.1007/s10913-004-0022-8.

Oreste, P. 2008. Distinct analysis of fully grouted bolts around a circular tunnel considering the congruence of displacements between the bar and the rock. *International Journal of Rock Mechanics and Mining Sciences,* 45(7), 1052-1067. Doi: https://doi.org/10.1016/j.ijrmms.2007.11.003.

Oreste, P. 2013. Face stabilization of deep tunnels using longitudinal fibreglass dowels. *International Journal of Rock Mechanics and Mining Sciences,* 58, 127-140. Doi: https://doi.org/10.1016/j.ijrmms.2012.07.011.

Oreste, P. and Peila, D. 1996. Radial passive rockbolting in tunnelling design with a new convergence-confinement model. *International Journal of Rock Mechanics and Mining Sciences & Geomechanics Abstracts,* 33(5), 443-454. Doi: https://doi.org/10.1016/0148-9062(96)00009-5.

Oreste, P. P. 2009. Face stabilisation of shallow tunnels using fibreglass dowels. *Proceedings of the Institution of Civil Engineers - Geotechnical Engineering,* 162(2), 95-109. Doi: https://doi.org/10.1680/geng.2009.162.2.95.

Oreste, P. P. and Cravero, M. 2008. An analysis of the action of dowels on the stabilization of rock blocks on underground excavation walls. *Rock mechanics and rock engineering,* 41(6), 835-868. Doi: https://doi.org/10.1007/s00603-008-0162-2.

Osgoui, R. R. and Oreste, P. 2007. Convergence-control approach for rock tunnels reinforced by grouted bolts, using the homogenization concept. *Geotechnical and Geological Engineering,* 25(4), 431-440. doi: https://doi.org/10.1007/s10706-007-9120-0.

Osgoui, R. R. and Oreste, P. 2010. Elasto-plastic analytical model for the design of grouted bolts in a Hoek–Brown medium. *International Journal for Numerical and Analytical Methods in Geomechanics,* 34(16), 1651-1686. Doi: https://doi.org/10.1002/nag.823.

Peila, I. D. and Oreste, I. P. P. 1995. Axisymmetric analysis of ground reinforcing in tunnelling design. *Computers and Geotechnics,* 17(2), 253-274. Doi: https://doi.org/10.1016/0266-352X(95)93871-F.

Pelizza, S., Peila, D. and Oreste, P. 1995. A new approach for ground reinforcing design in tunnelling. ed. *International Journal of Rock Mechanics and Mining Sciences and Geomechanics Abstracts*, 123A.

Ranjbarnia, M.*, et al.* 2016. Analytical-numerical solution for stress distribution around tunnel reinforced by radial fully grouted rockbolts. *International Journal for Numerical and Analytical Methods in Geomechanics,* 40(13), 1844-1862. Doi: https://doi.org/10.1002/nag.2517.

Ranjbarnia, M., Fahimifar, A. and Oreste, P. 2014. A simplified model to study the behavior of pre-tensioned fully grouted bolts around tunnels and to analyze the more important influencing parameters. *Journal of Mining science,* 50(3), 533-548. Doi: https://doi.org/10.1134/S1062739114030156.

Ranjbarnia, M., Fahimifar, A. and Oreste, P. 2015. Practical method for the design of pretensioned fully grouted rockbolts in tunnels. *International Journal of Geomechanics,* 16(1), 04015012. Doi: https://doi.org/10.1061/(ASCE)GM.1943-5622.0000464.

Ranjbarnia, M., Fahimifar, A., and Oreste, P. 2016. New analytical approaches for evaluating the performance of systematic pre-tensioned fully grouted rockbolts in tunnel stabilization. *Archives of Mining Sciences*, 61(4)., 823-852. Doi: https://doi.org/10.1515/amsc-2016-0056.

Ranjbarnia, M., Zaheri, M., and Dias, D. 2020. Three-dimensional finite difference analysis of shallow sprayed concrete tunnels crossing a reverse fault or a normal fault: A parametric study. *Frontiers of Structural and Civil Engineering*, 14(4), 998-1011. Doi: https://doi.org/10.1007/s11709-020-0621-8.

Stille, H., Holmberg, M. and Nord, G. 1989. Support of weak rock with grouted bolts and shotcrete. *International Journal of Rock Mechanics and Mining Sciences & Geomechanics Abstracts,* 26(1), 99-113. Doi: https://doi.org/10.1016/0148-9062(89)90530-5.

Tahmasebinia, F*., et al.* 2018. Numerical and analytical simulation of the structural behaviour of fully grouted cable bolts under impulsive loading. *International Journal of Mining Science and Technology,* 28(5), 807-811. Doi: https://doi.org/10.1016/j.ijmst.2018.08.012.

Teymen, A. 2017. Effect of mineral admixture types on the grout strength of fully-grouted rockbolts. *Construction and Building Materials,* 145, 376-382. Doi: https://doi.org/10.1016/j.conbuildmat.2017.04.046.

Wang, B., Zhao, F. J., and Peng, W. B. 2012. Numerical analysis for bolt length based on the stress response of anchorage surrounding rock. In *Applied Mechanics and Materials* , 204-208, 4481-4485. Doi: https://doi.org/10.4028/www.scientific.net/amm.204-208.4481.

Ward, W., Coats, D. and Tedd, P. 1976. Performance of tunnel support systems in the Four Fathom Mudstone. *Building Research Establishment. Garston, Watford, Current Paper CP 25/76,* (34630), 11.

Ward, W., Tedd, P. and Berry, N. 1983. The Kielder experimental tunnel: final results. *Geotechnique,* 33(3), 275-291. Doi: https://doi.org/10.1680/geot.1983.33.3.275.

Wu, K., Shao, Z., Li, C. and Qin, S. 2019. Theoretical investigation to the effect of bolt reinforcement on tunnel viscoelastic behavior. *Arabian Journal for Science and Engineering*, 45(5), 3707-3718. Doi: https://doi.org/10.1007/s13369-019-04215-9.

Xu, L. G., Li, H., Chen, X. L., and Chen, J. 2010. Numerical analysis on the impact of rock bolt parameters on stability of surrounding rock. *Chin J Geotech Eng*, *32*(S2), 249-252.

Zaheri, M., and Ranjbarnia, M. 2020. A New Procedure for Calculation of Ground Response Curve of a Circular Tunnel Considering the Influence of Young's Modulus

Variation and the Plastic Weight Loading. *Geotechnical and Geological Engineering*, 1-21. Doi: https://doi.org/10.1007/s10706-020-01546-5.

Zaheri, M., and Ranjbarnia, M. 2021. Ground reaction curve of a circular tunnel considering the effects of the altered zone and the self-weight of the plastic zones. *European Journal of Environmental and Civil Engineering*, 1-24. Doi: https://doi.org/10.1080/19648189.2021.1877829.

Zaheri, M., Ranjbarnia, M. and Oreste, P. 2019. Performance of systematic fully grouted rockbolts and shotcreted layer in circular tunnel under the hydrostatic conditions using 3D finite difference approach. *Geomechanics and Geoengineering*, 1-14. Doi: https://doi.org/10.1080/17486025.2019.1648885.

Zaheri, M., Ranjbarnia, M., and Dias, D. 2020a. 3D numerical investigation of segmental tunnels performance crossing a dip-slip fault. *Geomechanics and Engineering*, 23(4), 351-364. Doi: https://doi.org/10.12989/gae.2020.23.4.351.

Zaheri, M., Ranjbarnia, M., Dias, D., and Oreste, P. 2020b. Performance of segmental and shotcrete linings in shallow tunnels crossing a transverse strike-slip faulting. *Transportation Geotechnics*, *23*, 100333. Doi: https://doi.org/10.1016/j.trgeo.2020.100333.

Zhang, H., Lu, Y., and Cheng, Q. 2008. Numerical simulation of reinforcement for rock slope with rock bolt (anchor cable) frame beam. *Journal of Highway and Transportation Research and Development (English Edition)*, *3*(2), 65-71. Doi: https://doi.org/10.1061/JHTRCQ.0000247.

Zhu, C.*, et al.* 2015. Modeling of grout crack of rockbolt grouted system. *International Journal of Mining Science and Technology,* 25(1), 73-77. Doi: https://doi.org/10.1016/j.ijmst.2014.11.005.

Figures Captions:

Figure 1. Plane strain model constructed in FLAC^{2D} software

Figure 2. Simulation of the excavation phases

Figure 3. Schematic representation of the case of the study. Key: P_0: lithostatic pressure; P_i: internal support pressure; r_{in}: tunnel radius

Figure 4. The model constructed in FLAC^{3D} software

Figure 5. Application of the model to the Kielder Experimental Tunnel – Comparison between values of numerical modeling and the measured one

Figure 6. The effect of patterns of bolting and head constraint conditions on the radial displacements of the tunnel wall (u) a) B_1-BH, b) B_2-BH, c) B_1-FH, d) B_2-FH

Figure 7. Plastic band vs GSI a) fixed head constraint (BH), b) free head (FH)

Figure 8. Maximum axial force developed in the bolts (F_{max}) for the three considered P_0 a) B_1 scheme, b) B_2 scheme

Figure 9. Radial displacements of the tunnel wall vs GSI a) B_1-BH scheme, b) B_2-BH scheme

Figure 10. The effect of tunnel radius on F_{max} for various GSI and tunnel depths (B_1-BH scheme)

Figure 11. Plastic band vs GSI a) $R_T = 3$ m, b) $R_T = 6$ m (BH condition)

Figure 12. Tunnel displacements between two bolts

Figure 13. The influence of bolting density and the condition of the restraining of the head on the movement of tunnel wall on the bolt head location and in the middle of two bolt heads a) B_1-BH, b) B_2-BH, c) B_1-FH, d) B_2-FH

Figure 14. Radial displacements of the bolt head location and of the middle of two bolt heads for the two schemes of bolting a) B_1-BH scheme, b) B_2-BH scheme ($R_T = 6$ m)

Table 1. The 12 basic cases

Parameter	Unit	Values
GSI	-	35; 45; 55; 65
P_0	MPa	4; 8; 12

Table 2. GSI^{res} estimation from GSI^{peak} (Cai et al. 2007)

GSI^{peak}	GSI^{res}
75	35-45
70	30-40
60	28-37
50	25-33
40	23-30
30	21-27
25	20-25

Table 3. Characteristic parameters of the rock mass used in the calculations

	$GSI^{peak} = 35$	$GSI^{peak} = 45$	$GSI^{peak} = 55$	$GSI^{peak} = 65$
Elastic modulus (MPa)	2828	5808	11548	22497
Shear modulus (MPa)	1131	2323	4619	8998
Bulk modulus (MPa)	1885	3872	7699	14998
σ_{ci} (MPa)	45	60	75	90
m_b	0.687	0.982	1.403	2.006
s	0.0007	0.0022	0.0067	0.0205
GSI^{res}	24	27	30	33
m^{res}	0.4638	0.5162	0.5746	0.6396
s^{res}	0.0002	0.0003	0.0004	0.0006

Table 4. Bolting schemes

Parameter	B_1	B_2
Circumferential spacing (S_c)	1.2 m	0.6 m
Longitudinal spacing (S_l)	1 m	0.5 m

Table 5. Characteristic parameters of the bolting system for B_1 and B_2 schemes

Bolting schemes	Input Parameters						
	$\emptyset_m$ (°)	A_{bolt} (m^2)	P_{exp} (m)	$k_m \left(\frac{\frac{MN}{m}}{m}\right)$	S_m ($\frac{MN}{m^2}$)	E_{steel} (MPa)	R_t (MN)
B_1	38	0.0008	0.1728	32371	1.7279	21000	0.3539
B_2	38	0.0016	0.3456	64742	3.4557	42000	0.7077

Table 6. Comparison between the results obtained in FLAC^{2D} and FLAC^{3D} software programs (Data from Zaheri et al. 2019)

Cases	Displacement (m)		Plastic radius (m)	
	FLAC^{2D}	FLAC^{3D}	FLAC^{2D}	FLAC^{3D}
GSI ^{peak} = 25, σ_{ci} = 73.54 MPa, P_0 = 20.8 MPa	0.425	0.42	11	11
GSI ^{peak} = 60, σ_{ci} = 52.88 MPa, P_0 = 13 MPa	0.0068	0.007	7	7

Table 7. Rock mass strength parameters in section 2 of the tunnel (Ward et al. 1976, 1983)

Parameter	Unit	Value
GSI ^{peak}	-	35
σ_{ci}	MPa	37
m^{peak}	-	0.1
s^{peak}	-	0.00008
m^{res}	-	0.05
s^{res}	-	0.00001
v	-	0.25
Elastic modulus	MPa	5000
Shear modulus	MPa	2000
Bulk modulus	MPa	3333

Table 8. Bolting parameters (Freeman 1978; Ward et al. 1976, 1983)

Parameter	Unit	Value
Bolt length	m	1.8
Bolt diameter	m	0.025
Hole diameter	m	0.05
Grout thickness	m	0.0125
Section area of bolts	m^2	0.00049
Exposed perimeter	m	0.15708
Circumferential spacing between reinforcement elements (S_c)	m	0.9
Longitudinal spacing between reinforcement elements (S_l)	m	0.9
Elastic modulus of steel	MPa	210000
Compressive strength of grout	MPa	20
Shear modulus of grout	MPa	9000

Table 9. The Maximum axial forces developed in the bolts in the 48 cases under investigation

	Maximum axial force (MN) ($B_1 - BH$)		
GSI ^{peak}	$P_0 = 4$ MPa	$P_0 = 8$ MPa	$P_0 = 12$ MPa
35	0.3417	0.3539	0.3539
45	0.1584	0.3539	0.3539
55	0.05774	0.1815	0.3216
65	0.02968	0.05878	0.1218

	Maximum axial force (MN) ($B_2 - BH$)		
GSI ^{peak}	$P_0 = 4$ MPa	$P_0 = 8$ MPa	$P_0 = 12$ MPa
35	0.2283	0.35385	0.3539
45	0.1129	0.3075	0.3539
55	0.05395	0.1453	0.2624
65	0.02893	0.0565	0.1061

	Maximum axial force (MN) ($B_1 - FH$)		
GSI ^{peak}	$P_0 = 4$ MPa	$P_0 = 8$ MPa	$P_0 = 12$ MPa
35	0.3177	0.3539	0.3539
45	0.1104	0.3539	0.3539
55	0.0456	0.1405	0.2513
65	0.0256	0.0507	0.1028

	Maximum axial force (MN) ($B_2 - FH$)		
GSI ^{peak}	$P_0 = 4$ MPa	$P_0 = 8$ MPa	$P_0 = 12$ MPa
35	0.21845	0.35385	0.3539
45	0.11155	0.2923	0.3539
55	0.04986	0.1337	0.2515
65	0.02726	0.0531	0.097

* The red blanks show the cases in which the yield point is exceeded.

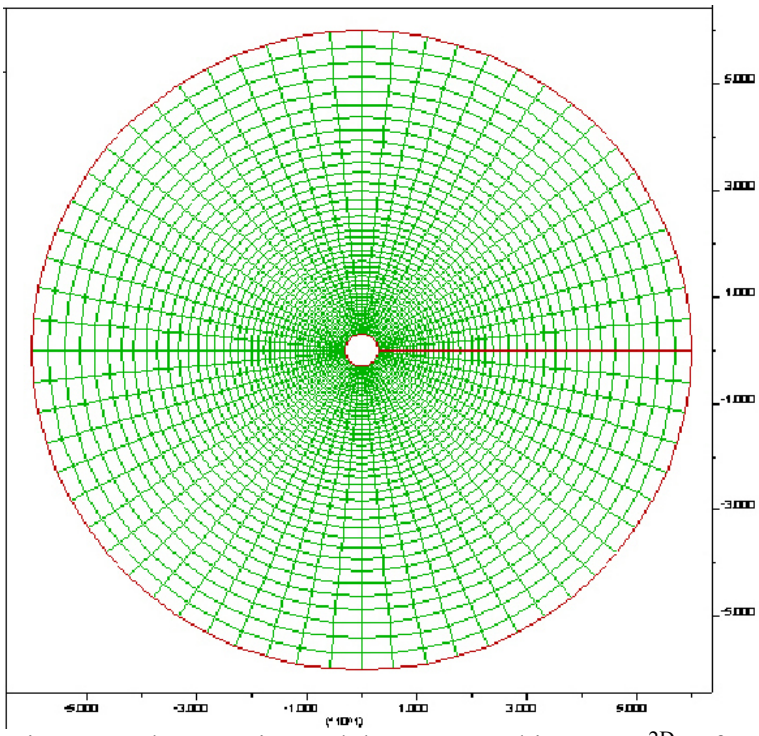

Figure 1. Plane strain model constructed in FLAC^{2D} software

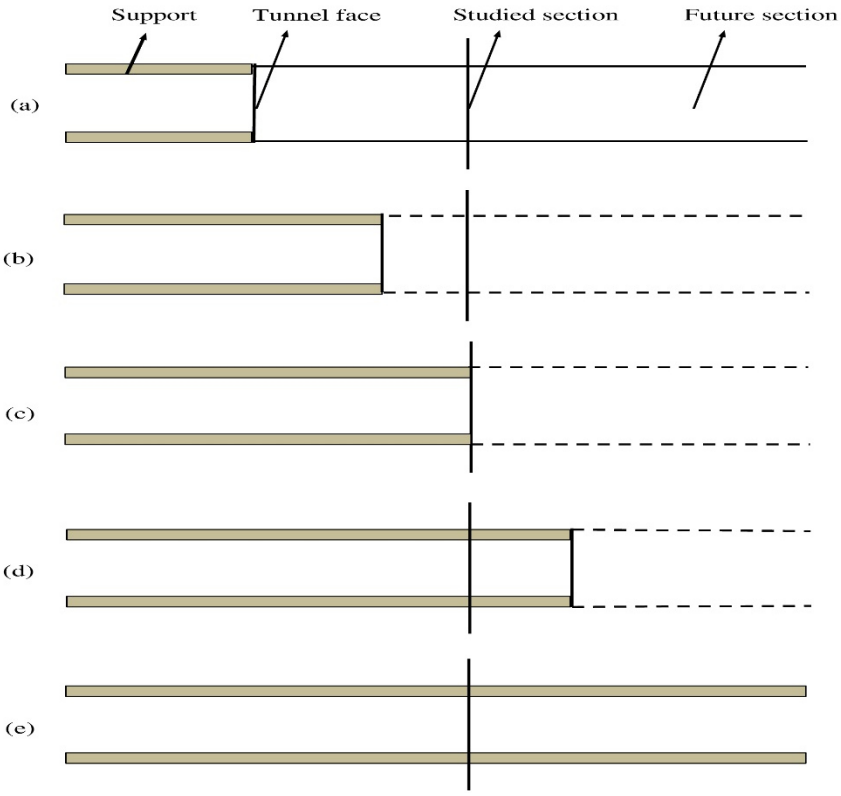

Figure 2. Simulation of the excavation phases

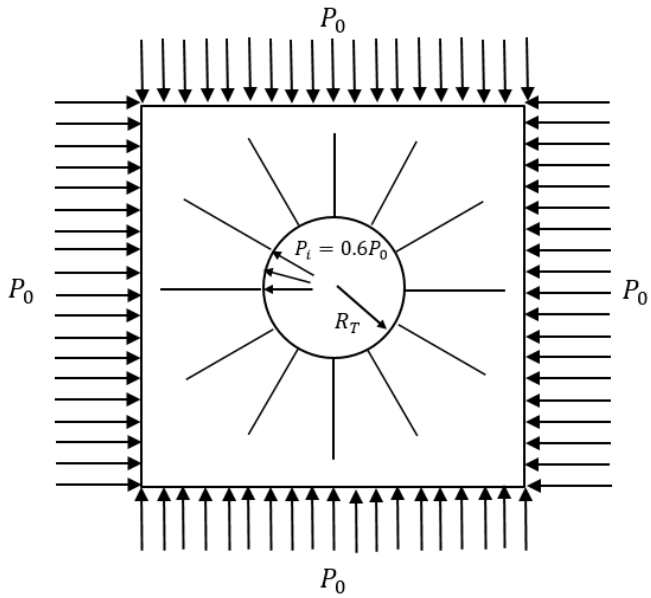

Figure 3. Schematic representation of the case of the study. Key: P_0: lithostatic pressure; P_i: internal support pressure; R_T: tunnel radius

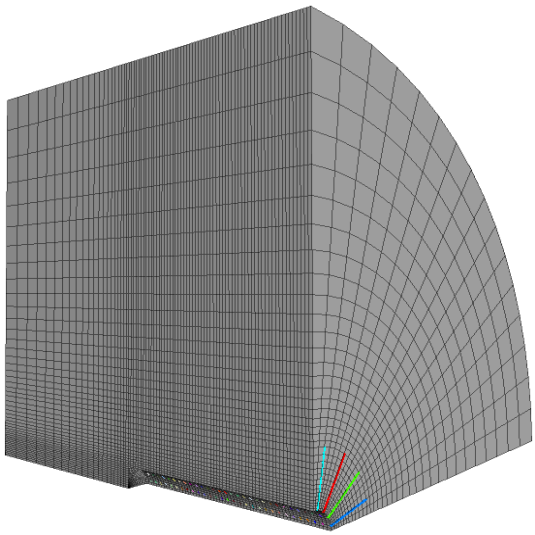

Figure 4. The model constructed in FLAC^{3D} software

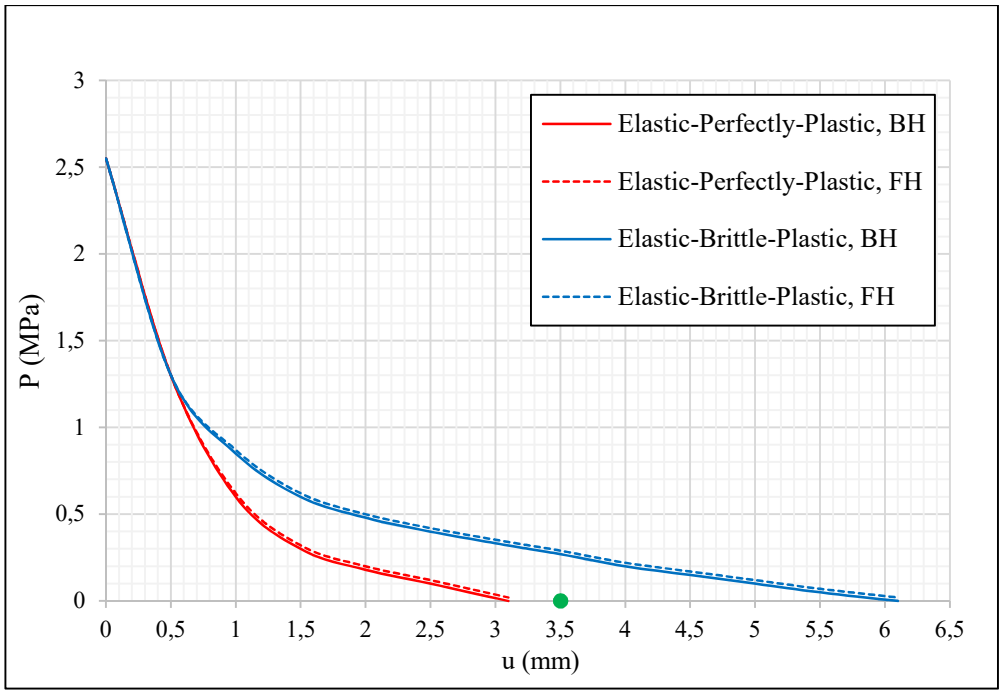

Figure 5. Application of the model to the Kielder Experimental Tunnel – Comparison between values of numerical modeling and the measured one

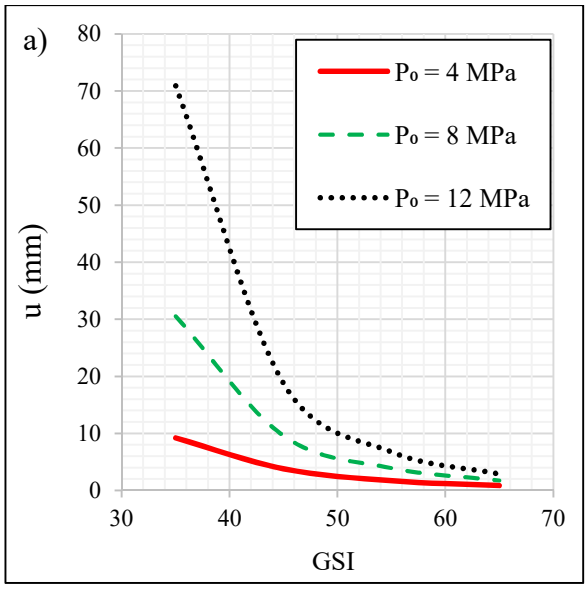
a)
u (mm)
GSI
P₀ = 4 MPa
P₀ = 8 MPa
P₀ = 12 MPa
0
10
20
30
40
50
60
70
80
30
40
50
60
70

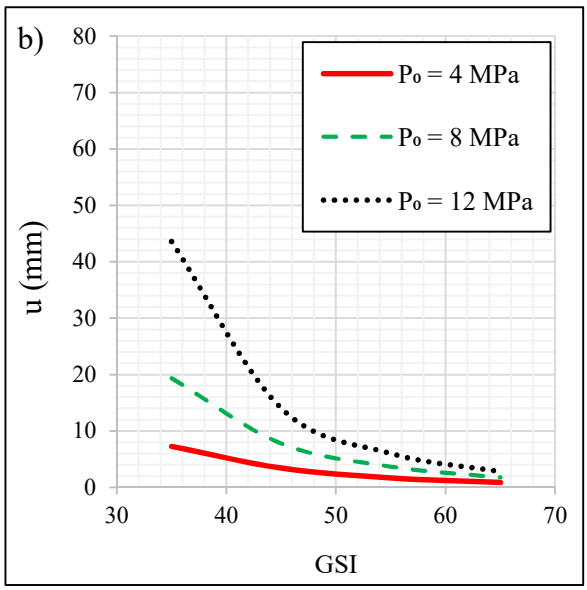
b)
u (mm)
GSI
P₀ = 4 MPa
P₀ = 8 MPa
P₀ = 12 MPa
0
10
20
30
40
50
60
70
80
30
40
50
60
70

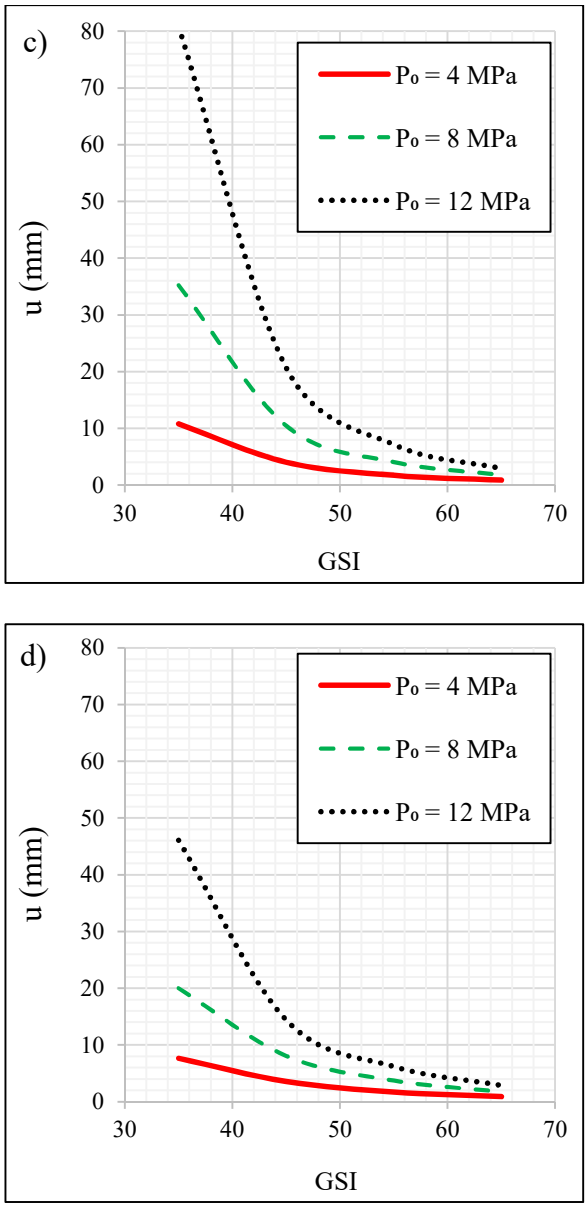

Figure 6. The effect of patterns of bolting and head constraint conditions on the radial displacements of the tunnel wall (u) a) B_1-BH, b) B_2-BH, c) B_1-FH, d) B_2-FH

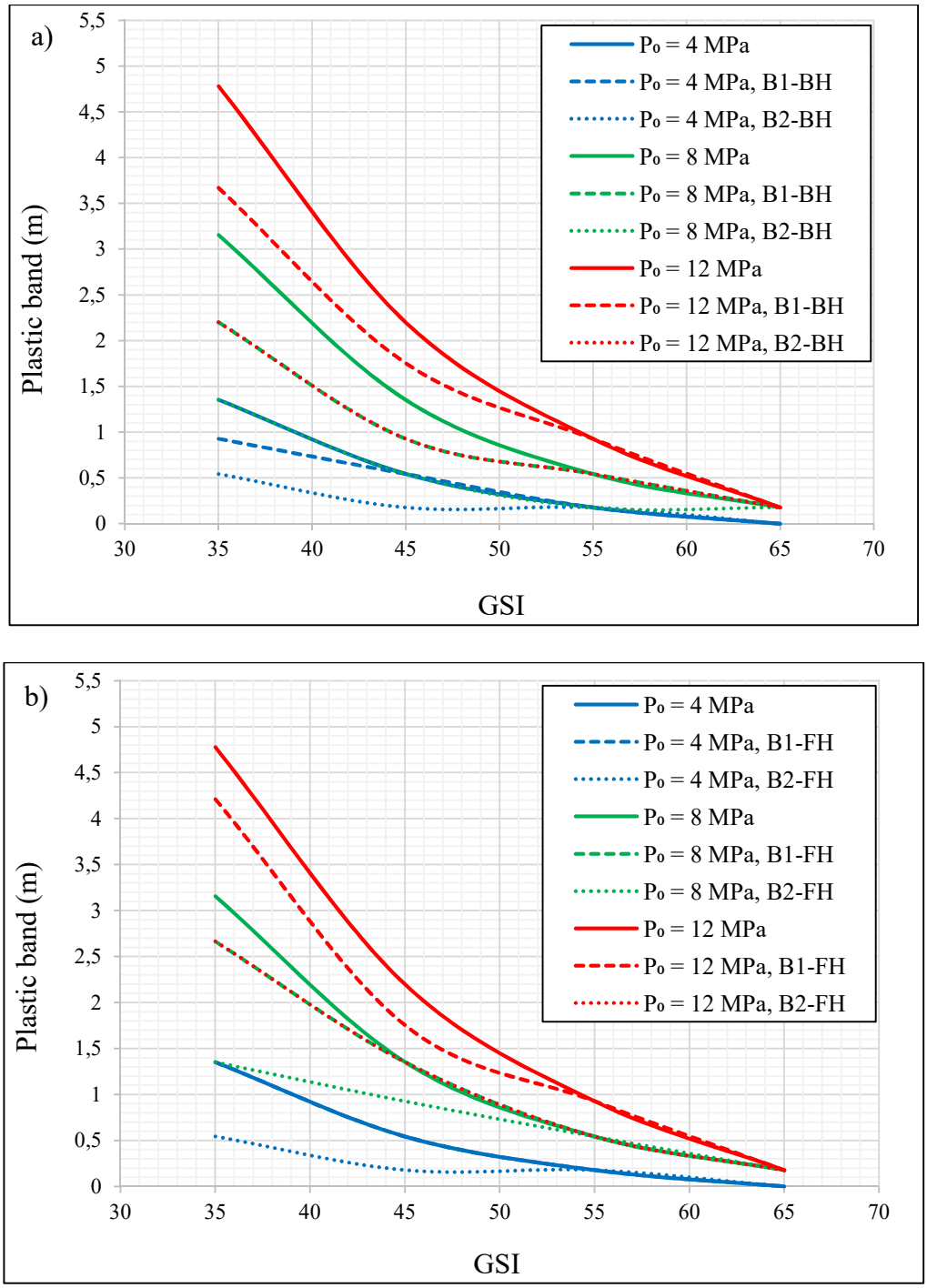

Figure 7. Plastic band vs GSI a) fixed head constraint (*BH*), b) free head (*FH*)

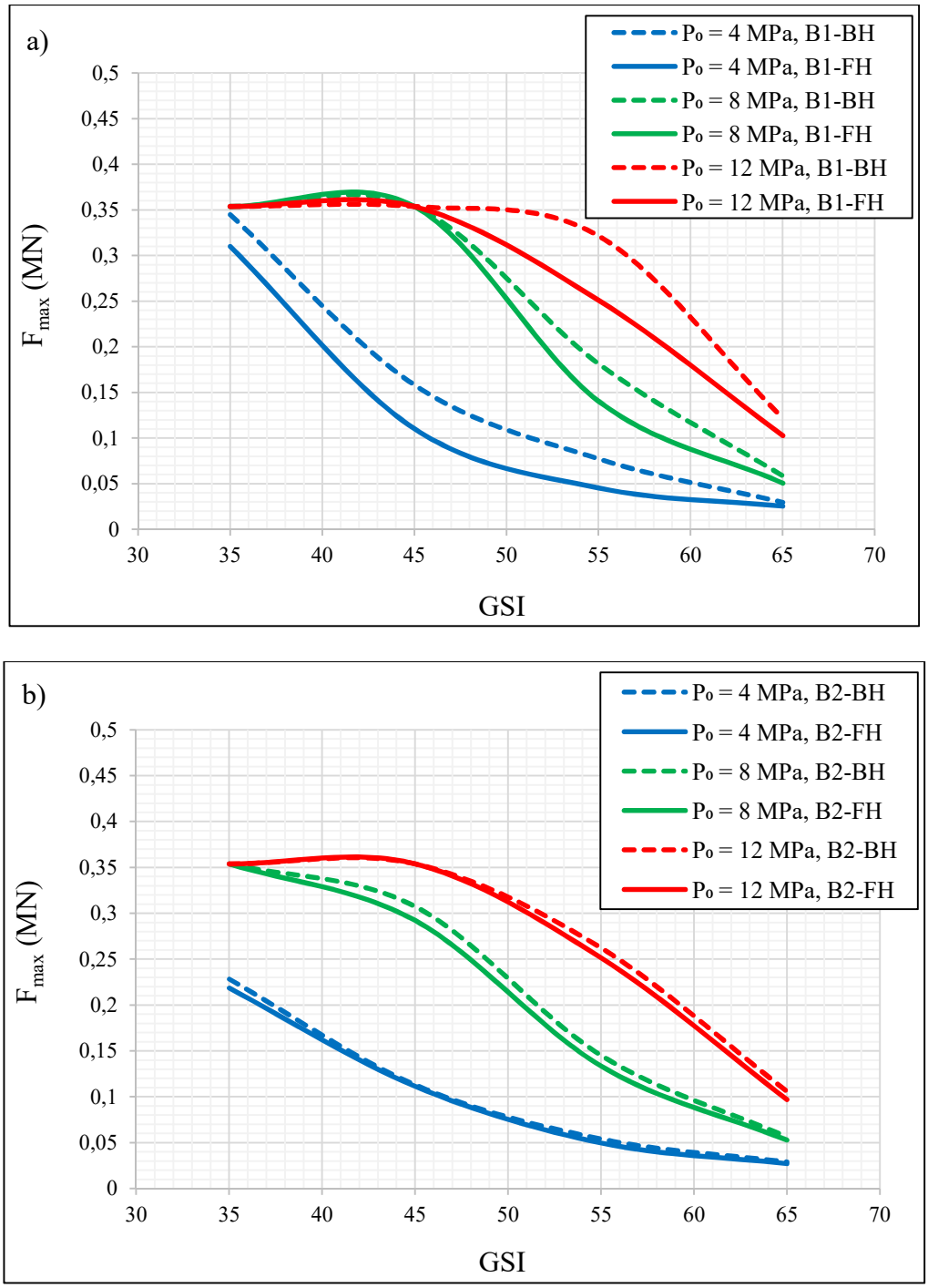

Figure 8. Maximum axial force developed in the bolts (F_{max}) for the three considered P_0 a) B_1 scheme, b) B_2 scheme

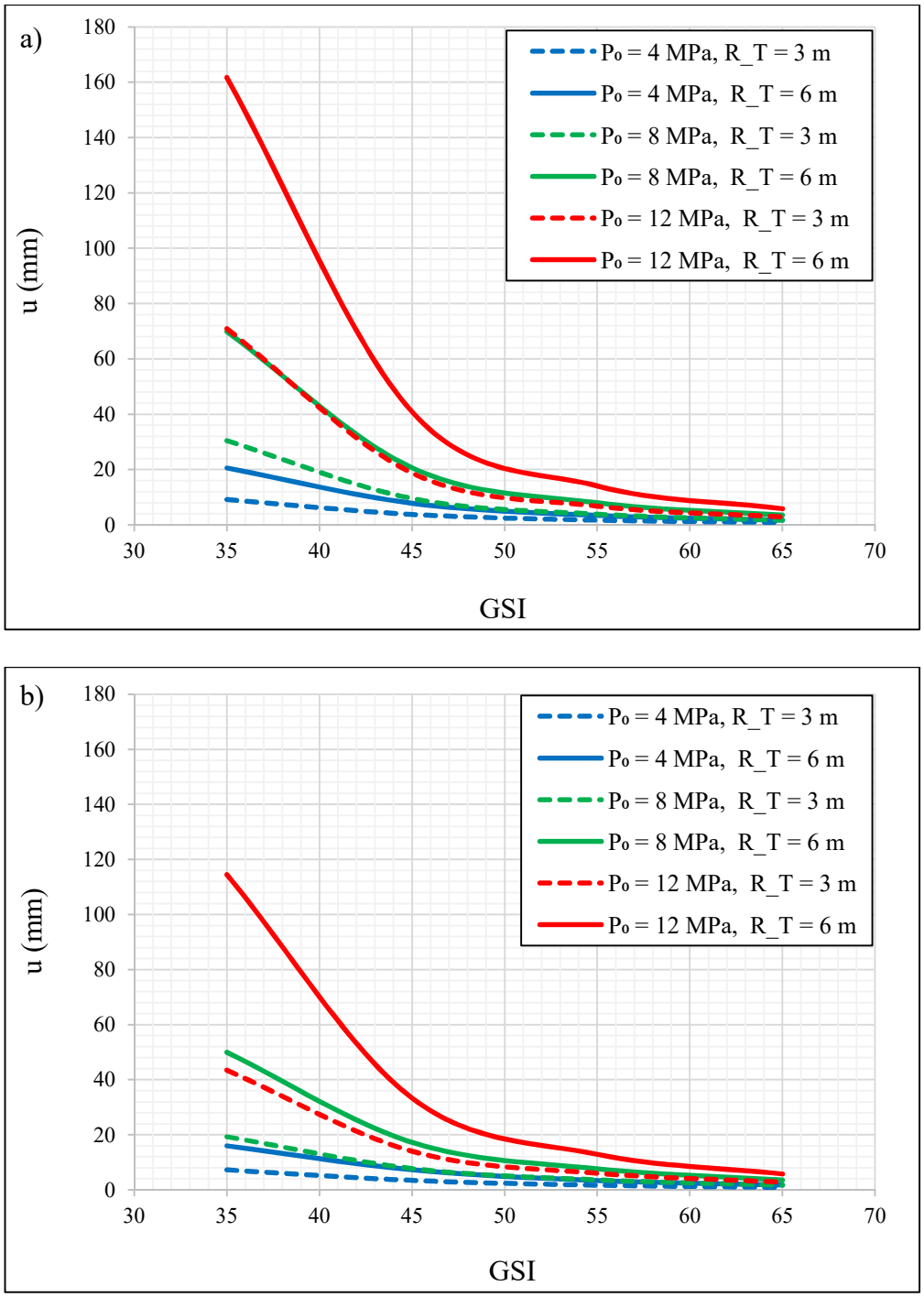

Figure 9. Radial displacements of the tunnel wall vs GSI a) B_1-*BH* scheme, b) B_2-*BH* scheme

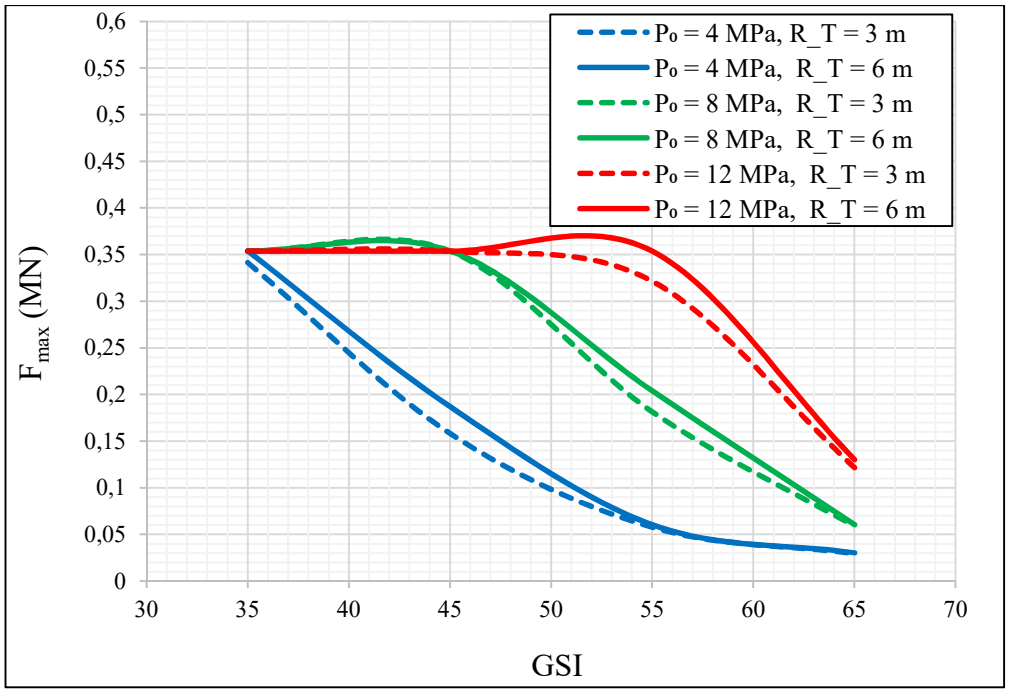

Figure 10. The effect of tunnel radius on F_{max} for various GSI and tunnel depths (B_1-*BH* scheme)

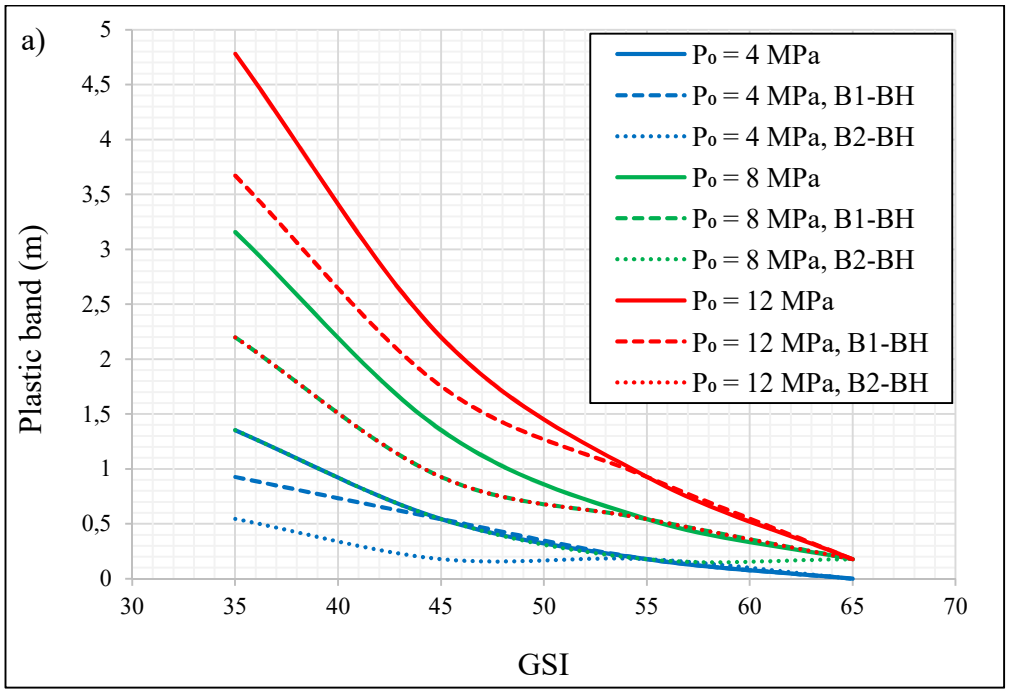

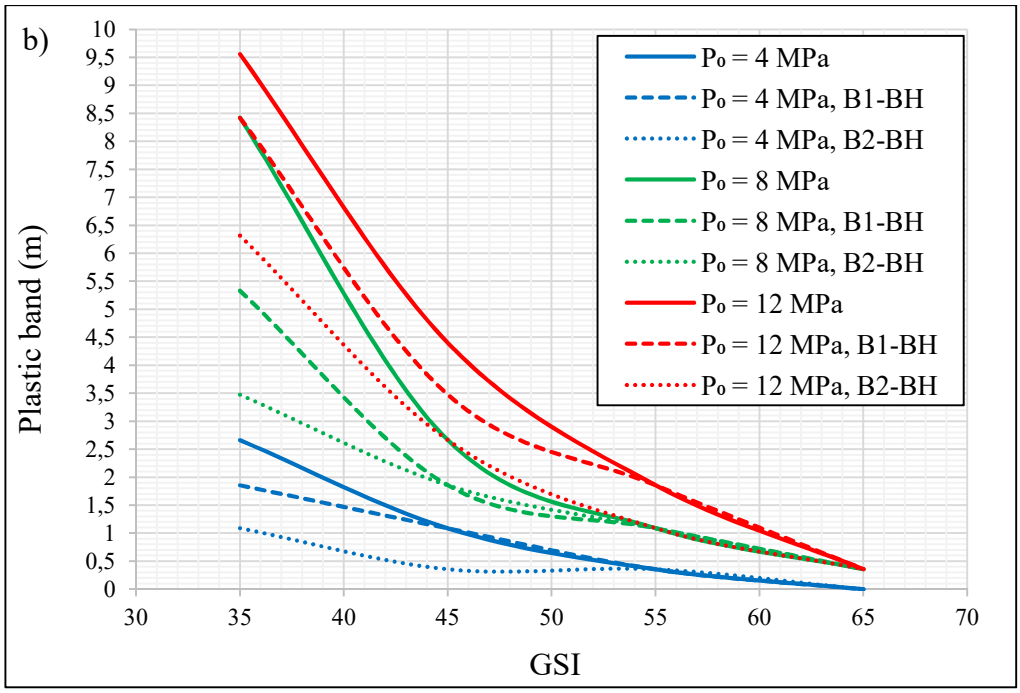

Figure 11. Plastic band vs GSI a) $R_T = 3$ m, b) $R_T = 6$ m (*BH* condition)

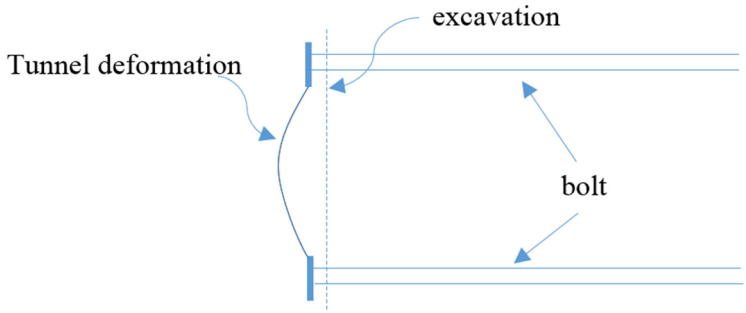

Figure 12. Tunnel displacements between two bolts

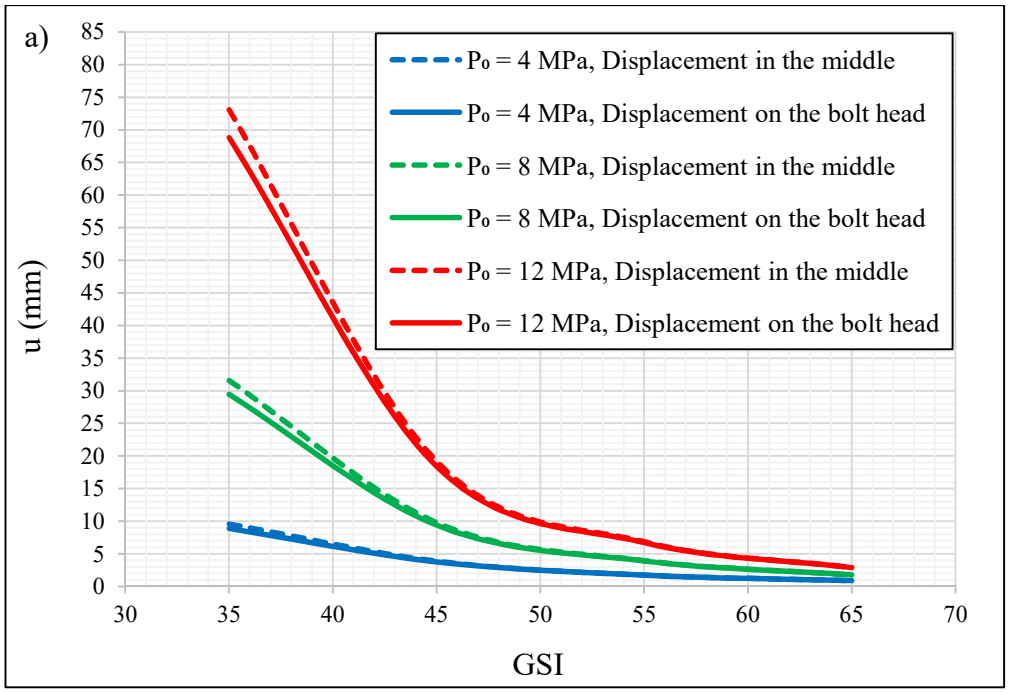
a)
u (mm)
GSI
P₀ = 4 MPa, Displacement in the middle
P₀ = 4 MPa, Displacement on the bolt head
P₀ = 8 MPa, Displacement in the middle
P₀ = 8 MPa, Displacement on the bolt head
P₀ = 12 MPa, Displacement in the middle
P₀ = 12 MPa, Displacement on the bolt head

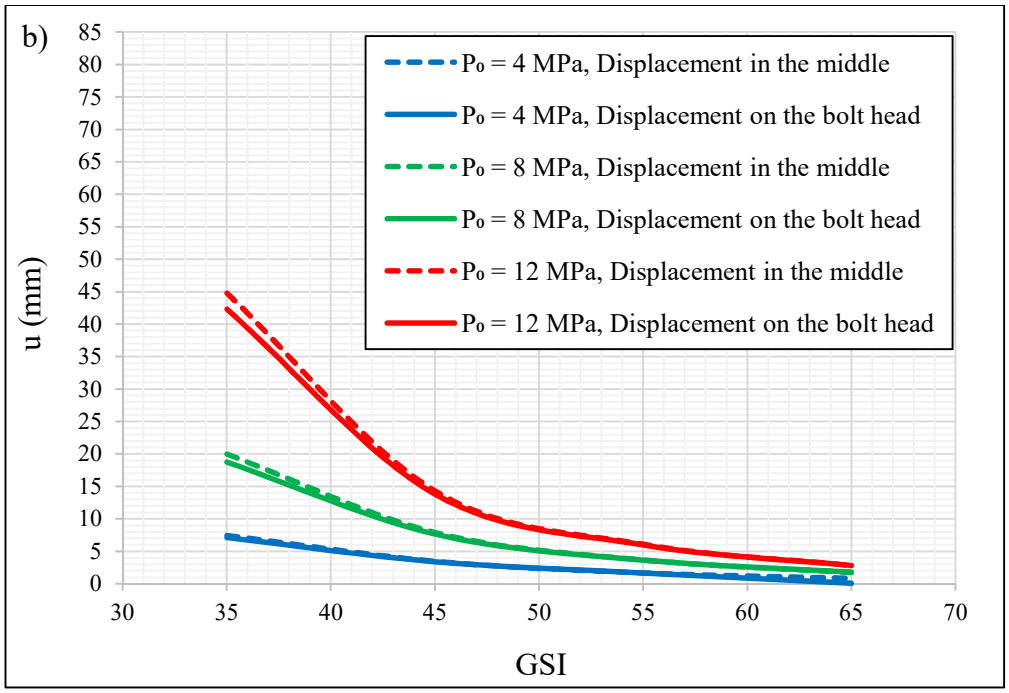
b)
u (mm)
GSI
P₀ = 4 MPa, Displacement in the middle
P₀ = 4 MPa, Displacement on the bolt head
P₀ = 8 MPa, Displacement in the middle
P₀ = 8 MPa, Displacement on the bolt head
P₀ = 12 MPa, Displacement in the middle
P₀ = 12 MPa, Displacement on the bolt head

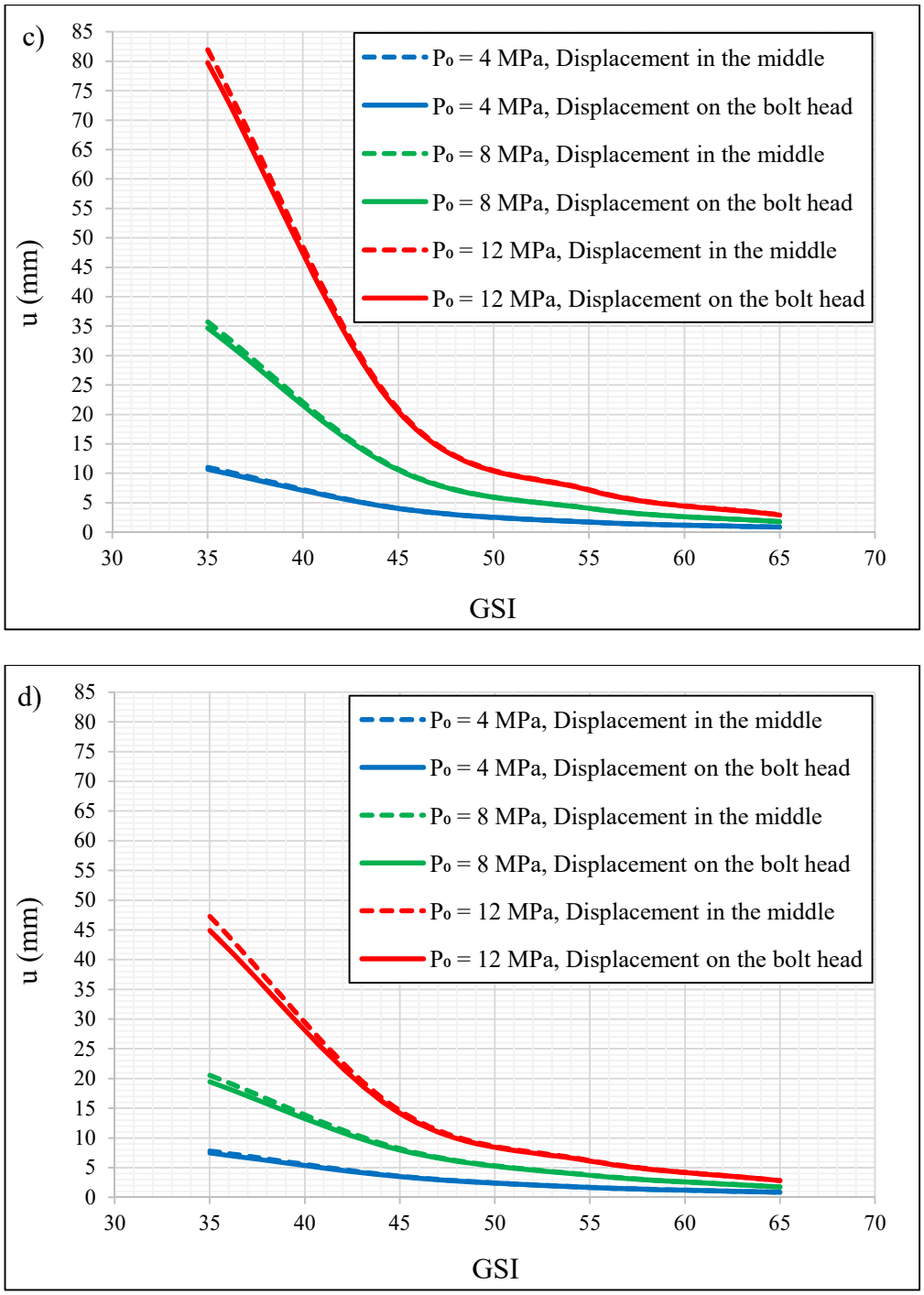

Figure 13. The influence of bolting density and the condition of the restraining of the head on the movement of tunnel wall on the bolt head location and in the middle of two bolt heads a) B_1-*BH*, b) B_2-*BH*, c) B_1-*FH*, d) B_2-*FH*

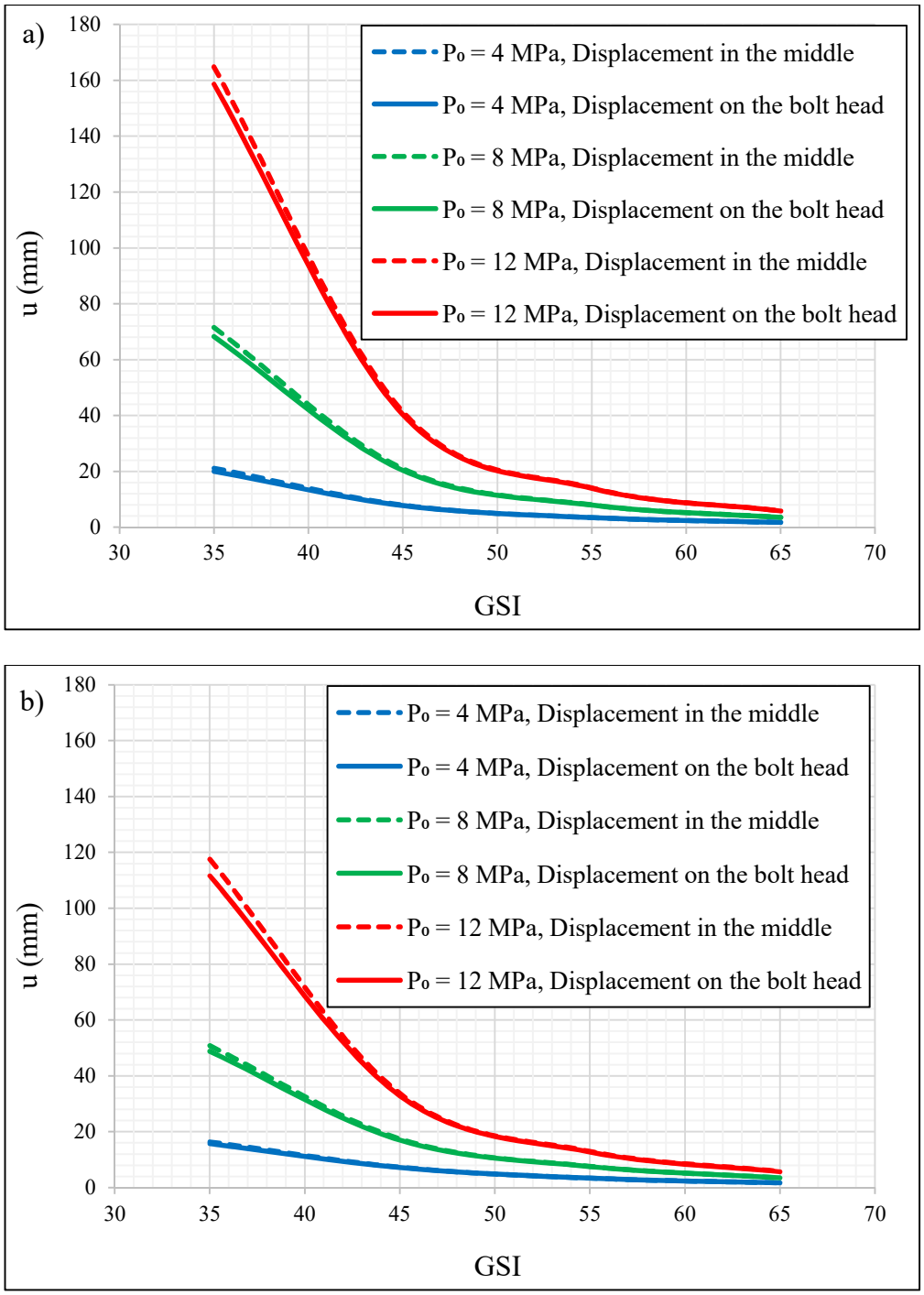

Figure 14. Radial displacements of the bolt head location and of the middle of two bolt heads for the two schemes of bolting a) B_1-BH scheme, b) B_2-BH scheme ($R_T = 6$ m)